1386 *Chem. Mater.* **1998,** *10,* 1386−1395

Reversed (Negative) Magnetization for Electrochemically Deposited High-T_c Thin Films of Chromium Hexacyanide Magnets

Wayne E. Buschmann,[1a] Scott C. Paulson,[1a] Charles M. Wynn,[1b]
Mihai A. Girtu,[1b] Arthur J. Epstein,*[,1b,c] Henry S. White,*[,1a] and
Joel S. Miller*[,1a]

The Department of Chemistry, University of Utah, Salt Lake City, Utah 84112-0850, and the Department of Physics and Department of Chemistry, The Ohio State University, Columbus, Ohio 43210-1106

Received November 25, 1997. Revised Manuscript Received February 19, 1998

Thin films of chromium cyanide Prussian blue-like materials, $K_nCr_x[Cr(CN)_6]$ (ca. 1.0 ± 0.5 μm thick) are electrodeposited on glassy carbon electrodes in amorphous (a) and crystalline (α) forms. The crystalline film shows a X-ray diffraction pattern typical of a face-centered cubic (fcc) Prussian blue-type cubic lattice [$a = 10.41(2)$ Å]. The films exhibit quasi-reversible cyclic voltammetric waves, distinct morphologies in SEM images, and strong field-dependent magnetic behavior. The films undergo two one-electron processes, $Cr^{II}[Cr^{II}(CN)_6]^{2-} \rightleftharpoons Cr^{III}[Cr^{II}(CN)_6]^- + e^-$, and $Cr^{III}[Cr^{II}(CN)_6]^- \rightleftharpoons Cr^{III}[Cr^{III}(CN)_6] + e^-$, with some residual Cr^{II} being present. The composition is determined from an analysis of the υ_{CN} IR data {$[Cr^{II}(CN)_6]^{4-}$: $\upsilon_{CN} = 2072$s cm^{-1}; $[Cr^{III}(CN)_6]^{3-}$: $\upsilon_{CN} = 2185$m cm^{-1}} and X-ray photoelectron (XPS) spectral data. The composition of the oxidized and reduced films are $Cr^{III}[Cr^{III}(CN)_6]_{0.98}[Cr^{II}(CN)_6]_{0.02}$ and $K_{2.0}Cr^{II}[Cr^{II}(CN)_6]$, respectively, for both amorphous and crystalline forms. These materials exhibit broad intervalence charge-transfer bands in their oxidized [$\lambda_{max} = 18\,800$ cm^{-1} ($\epsilon \sim 1280$ cm^{-1} M^{-1}); 35 500 cm^{-1} ($\epsilon \sim 1180$ cm^{-1} M^{-1})] and reduced [$\lambda_{max} = 20\,200$ cm^{-1} ($\epsilon \sim 870$ cm^{-1} M^{-1}); 36 700 cm^{-1} ($\epsilon \sim 770$ cm^{-1} M^{-1})] forms. The crystal field splitting Δ_o's for $Cr^{II}(NC)_6$ and $Cr^{III}(NC)_6$ are 19 500 and 26 600 cm^{-1}, respectively. The magnetic ordering temperatures, T_c, are a function of Cr oxidation state and range between 135 and 260 K for both film types. The T_c's are independent of crystallinity, suggesting that the magnetic domains are smaller than the short-range structural order for both a- and α-films. Hysteresis is observed for the films, with coercive fields as high as 830 Oe at 20 K, confirming the existence of bulk ferrimagnetic behavior below T_c. We determined that the coercivity of the amorphous films is larger than that of the crystalline films and suggest that this due to the larger number of defects in the a-films.

Introduction

Recent efforts have focused on developing molecule-based materials that possess bulk magnetic order near or above room temperature.[2−5] One class of such materials, albeit more like akin to 3-D network oxides, are mixed-valent metal hexacyanide systems possessing the Prussian blue face-centered cubic lattices.[4,5] In the ideal case this structure type has $-M-C{\equiv}N-M'-N{\equiv}C-M-$ repeat units along all three crystallographic axes. The magnetic coupling and ordering temperatures can be varied through the use of different combinations of metals (M and M′) and/or their oxidation states. Examples of compounds with the highest magnetic ordering temperatures, T_c, contain early transition metals and include $Cr^{II}_{1.5}[Cr^{III}(CN)_6]\cdot 5H_2O$ (**1**, $T_c = 240$ K)[5] and the room-temperature magnet $V[Cr(CN)_6]_{0.86}\cdot 2.8H_2O$ ($T_c = 315$ K).[4c] The magnetic behavior is attributed to the strong antiferromagnetic coupling

---

(1) (a) University of Utah. (b) Department of Physics, The Ohio State University. (c) Department of Chemistry, The Ohio State University.

(2) (a) Manriquez, J. M.; Yee, G. T.; McLean, R. S.; Epstein, A. J.; Miller, J. S. *Science* **1991**, *252*, 1415. (b) Miller, J. S.; Yee, G. T.; Manriquez, J. M.; Epstein, A. J. In the Proceedings of Nobel Symposium #NS-81, *Conjugated Polymers and Related Materials: The Interconnection of Chemical and Electronic Structure*; Oxford University Press: Oxford, 1993; p 461. (c) Epstein, A. J.; Miller, J. S. In the Proceedings of Nobel Symposium #NS-81, *Conjugated Polymers and Related Materials: The Interconnection of Chemical and Electronic Structure*; Oxford University Press: Oxford, 1993; p 475. (d) Zhang, J.; Zhou, P.; Brinckerhoff, W. B.; Epstein, A. J.; Vazquez, C.; McLean, R. S.; Miller, J. S. *Am. Chem. Soc., Symp. Ser.* **1996**, *644*, 311.

(3) Miller, J. S.; Epstein, A. J. *Angew. Chem.* **1994**, *33*, 385. Miller, J. S.; Epstein, A. J. *Chem. Eng. News* **1995**, *73* (No. 40), 30. Kinoshita, M. *Jpn. J. Appl. Phys.* **1994**, *33*, 5718. Kahn, O. *Molecular Magnetism*; VCH Publishers: New York, 1993. Gatteschi, D. *Adv. Mater.* **1994**, *6*, 635. *Molecule-based Magnets*; Miller, J. S., Epstein, A. J., Eds.; *Mol. Cryst. Liq. Cryst.* **1995**, *271−274*. *Molecular Assemblies to the Devices: NATO Advanced Studies Workshop*; Coronado, E., Delhaès, P., Gatteschi, D., Miller, J. S., Eds.; Kluwer Academic Publishers: London, 1996; *E321. Molecule-based Magnetic Materials*; Turnbull, M. M., Sugimoto, T., Thompson, L. K. *Am. Chem. Soc., Symp. Ser.* **1967**, 644. *Molecular-Based Magnets*; Itoh, K., Takui, T., Miller, J. S., Eds. *Mol. Cryst. Liq. Cryst.* **1997**, *305−306*.

(4) (a) Gadet, V.; Mallah, T.; Castro, I.; Verdaguer, M. *J. Am. Chem. Soc.* **1992**, *114*, 9213. (b) Entley, W. R.; Girolami, G. *Science* **1995**, *268*, 397. (c) Ferlay, S.; Mallah, T.; Ouahes, R.; Veillet, P.; Verdaguer, M. *Nature* **1995**, *378*, 701.

(5) Mallah, T.; Thiébaut, S.; Verdaguer, M.; Veillet P. *Science* **1993**, *262*, 1554.

Table 1. Summary of the Magnetic Properties of Chromium Cyanide Prussian Blue Structured Materials

	θ, K	T_c, K	M_s, emu Oe/mol	H_{cr}, Oe[a]	ref
$Cr^{II}_{1.5}[Cr^{III}(CN)_6]\cdot 5H_2O$	−306	240	7820[b]	20	5
$Cs_{0.75}Cr^{II}_{1.125}Cr^{III}(CN)_6\cdot 5H_2O$	−440	190	5300[b]	[c]	5
$Cr^{II}_{1.29}Cr^{III}_{1.14}(CN)_6\cdot 6.09H_2O$	−320	240	3910[d]	25	6
$Cr^{II}_{0.36}Cr^{III}_{1.76}(CN)_6\cdot 2.8H_2O$	−416	270	2790[d]	143	6
$Cs_{1.15}Cr^{II}_{1.33}Cr^{III}_{0.73}(CN)_6\cdot 1.78H_2O$	−119	150	3910[d]	130	6

[a] 5 K. [b] At 7 T and 10 K. [c] Not reported. [d] At 5 T and 10 K.

between adjacent metal sites through the antibonding orbitals of the bridging cyanide ligands.[4c,5,6]

These insoluble, Prussian blue structured materials are prepared as bulk solids. This method, however, is restricted to available starting materials and hence limits available oxidation states. An alternative to producing bulk precipitates is to deposit thin films by electrochemical methods. $\{Fe^{III}_x[Fe^{II}(CN)_6]\}^{z-}$,[7a] $\{Cr^{III}_x[Fe^{II}(CN)_6]\}^{z-}$,[7b] $\{Co^{II}_x[Fe^{II}(CN)_6]\}^{z-}$,[7c] and recently $\{Cr_x[Cr(CN)_6]\}^{z-}$ (**2**),[6] have been electrochemically deposited onto electrode surfaces. For **2**, advantage is taken of the substitutionally inert $[Cr^{III}(H_2O)_6]^{3+}$, which is electrochemically reduced to Cr^{II} and then rapidly precipitates as $Cr^{II}_x[Cr^{III}(CN)_6]_y$. Thin films of these mixed-valent chromium compounds have T_c's between 100 and 270 K depending upon the electrochemically controlled oxidation state.[6] Films of $Cs_{2.43}Cr_{2.06}(CN)_6\cdot 1.78H_2O$, $Cr_{2.12}(CN)_6\cdot 2.80H_2O$, and $Cr_{2.43}(CN)_6\cdot 6.09H_2O$[6] have also been electrochemically deposited onto indium-doped tin oxide (ITO) electrodes and the bulk syntheses of $Cs_{0.75}Cr_{2.125}(CN)_6\cdot 5H_2O$ and $Cr_{1.5}[Cr(CN)_6]\cdot 5H_2O$[5] have been reported (Table 1).

Herein, we describe the synthesis, characterization, and magnetic properties of chromium cyanide-based electrodeposited films on glassy carbon (GC) and indium-doped tin oxide (ITO) electrodes. The focus of this work is to understand the effect of the Cr^{II}:Cr^{III} ratio and morphology on the magnetic properties, not to optimize the T_c by varying the Cr^{II}:Cr^{III} ratio. Physical measurements were made with the films intact on the electrode surface. Two distinct film types, amorphous (a-phase) and crystalline (α-phase), with differing morphology and magnetic behaviors were formed. The T_c and coercive fields of the films depend on the ratio of Cr^{II}:Cr^{III}, which can be reversibly varied by electrochemical methods.

Experimental Section

$[Cr(H_2O)_6]Cl_3$ (Allied Chemical), KCl, potassium acetate (Fisher Scientific), tetra-*n*-butylammonium chloride (Aldrich), and methanol (<0.01% H_2O, Mallinckrodt) were reagent grade and used as received. Aqueous solutions were prepared with water purified through a Barnstead "E-pure" water purification system, and the solutions were bubbled with N_2 for 2 h and confirmed to be O_2-free by dissolving $V^{II}(SO_4)$ without oxidation. Pale yellow $K_3[Cr(CN)_6]$ ($\upsilon_{CN} = 2093$ cm^{-1}) was prepared by oxidizing a methanolic suspension of $K_4[Cr(CN)_6]$[8a] by air exposure until the 2026 cm^{-1} $\upsilon_{Cr^{II}CN}$ absorption could not be detected.[8b] Elemental analysis for $K_3Cr(CN)_6$: calcd (found) C, 22.15 (22.25)%; H, 0.00 (0.16)%; N, 25.83 (25.65)%.

Working electrodes were prepared from glassy carbon (GC; Alfa Aesar, type 1) and highly oriented pyrolytic graphite (HOPG; Advanced Ceramics Corp., Cleveland, OH). The GC electrodes were either rods (2- and 7-mm diameter) or disks cut from a 7-mm-diameter rod. The GC rods were periodically cleaned in a sonic bath with high-purity water and methanol while the disks were periodically polished with 10 μm alumina powder (Alfa Aesar). The HOPG surface was prepared by removing the top surface layer with adhesive tape. Both the basal and edge planes of the HOPG electrode were exposed to the electrochemical solutions.

Electrochemical measurements were made using a conventional three-electrode cell equipped with a Pt wire counter electrode and an aqueous Ag/AgCl (saturated KCl) reference electrode. Voltammetric curves were obtained using a Bioanalytical Systems Model CV-27 potentiostat or an EG&G Princeton Applied Research Model 273 potentiostat. Electrochemistry was performed at room temperature in an in-house-built N_2 atmosphere "wetbox" and a Vacuum Atmospheres DriLab lacking molecular sieves. Preparation of nonaqueous solutions as well as sample weightings were performed in a Vacuum Atmospheres inert atmosphere DriLab.

Infrared (IR) spectra were recorded on a Mattson Galaxy series 3000 FTIR spectrophotometer. IR studies were made using a 25-mm-diameter × 2-mm-thick CaF_2 disk (Wilmad) coated with an ITO film ($R_s = 10-50$ Ω/sq, Metavac, Inc.). Thin films of $K_nCr_x[Cr(CN)_6]$ were electrochemically deposited on the ITO surface. The electrochemical cell was designed using two concentric glass tubes, the outer capped with the ITO-coated CaF_2 window and the inner capped with a plain CaF_2 window. The inner tube was sealed to the outer tube with an O-ring adapter. The counter (Pt wire) and reference (Ag wire) electrodes were fed through the outer tube wall. Nujol mull IR spectra were also taken of samples that were scraped off the surface of a 7 mm GC rod after electrodeposition. Peak area integrations were made using the Win-First IR software provided by Mattson.

UV−vis−NIR spectra (250−1900 nm) were made using a Cary-17D spectrophotometer equipped with an On-Line Instrument Systems Inc. interface. Solution spectra were measured in an 1 cm gastight quartz cuvette in O_2-free water. Spectra of $K_nCr_x[Cr(CN)_6]$ films were obtained using films deposited onto ITO-coated fused quartz slides ($R_s \leq 100$ Ω/sq, Delta Technologies, Ltd.). The electrodes were cycled to the appropriate potential in a fresh 0.2 M KCl solution, briefly dried under a pure nitrogen purge, and contained in an airtight quartz cell. Molar absorptivities for the films were determined assuming a Beer's law relationship. The concentration of the material was based on the density derived from unit cell and estimated formula weight. The path length (thickness of a uniform film) was calculated from the electrode area, density, and film mass.

X-ray photoelectron spectra (XPS) were obtained using a Fisons ESCALAB, Model 220i-XL spectrometer, with an Al Kα radiation source operated at 10 kV and 15 mA. High-resolution scans were measured using a band-pass energy of 20 eV. The X-ray beam was focused to a 100-μm-diameter spot size, while a 6−8 eV electron flood gun was used to control charging on the samples. System pressures were $\sim 7 \times 10^{-12}$ bar. XPS spectra at different locations on the films demonstrated a uniform composition. The $K_nCr_x[Cr(CN)_6]$ films for XPS analysis were prepared using 7-mm-diameter GC disks. After rinsing the electrode surface with water, the electrodes were transferred under N_2 by a special transfer arm that

---

(6) Sato, O.; Iyoda, T.; Fujishima, A.; Hashimoto, K. *Science* **1996**, *271*, 49.

(7) (a) Kulesza, P. J.; Doblhofer, K. *J. Electroanal Chem.* **1989**, *274*, 95. (b) Gao, Z. *J. Electroanal. Chem.* **1994**, *370*, 95. (c) Kulesza, P. J.; Malik, M. A.; Miecznikowski, K.; Wolkiewicz, A. *J. Electrochem. Soc.* **1996**, *143*, L10.

(8) (a) Christensen, O. T. *J. Prakt. Chem.* **1885**, *31*, 163. (b) Mallah, T.; Verdaguer, M., personal communication.

allowed direct, O_2-free loading of the sample into the spectrometer. Samples were then degassed at ~1 × 10^{-12} bar for up to 12 h before measurement. The carbon 1s peak of the glassy carbon substrate (284.6 eV) was used to normalize the energy shift of the spectra.

Scanning electron microscopy (SEM) was performed on a Cambridge Instruments Model S240 using a LaB_6 filament source. Accelerating voltages are noted in figure captions. The $K_nCr_x[Cr(CN)_6]$ films for SEM analysis were deposited on 7-mm-diameter GC disks. The GC disks were mounted on aluminum holders with double-sided conducting tape.

X-ray powder diffraction spectra were taken on a Rigaku Model 1GC2 Miniflex diffractometer using Cu Kα radiation. The reflection 2θ values were corrected using an internal crystalline silicon standard and refinements made using a VAX-based refinement program, LATPARM. The films for this analysis were deposited on 7-mm-diameter GC disks as described above, which were adhered to either glass slides or on an aluminum holder. Powder samples were mounted on glass slides.

Electron paramagnetic resonance (EPR) spectra were obtained with a Bruker Model ESP 300E spectrometer equipped with an X-band microwave bridge with a Model ER 041 XK frequency counter and an Oxford He cryostat controller. Measurements were made on $K_nCr_x[Cr(CN)_6]$ films that were deposited onto 1- and 2-mm-diameter × 9-mm-long GC rods contained in standard fused-quartz EPR tubes.

Magnetic susceptibility measurements (20−300 K) were made using a Quantum Design MPMS-5 5T SQUID magnetometer with a sensitivity of 10^{-8} emu (or 10^{-12} emu/Oe at 1 T) and equipped with the ultralow field (~0.005 Oe) option, reciprocating sample measurement system, and continuous low-temperature control with enhanced thermometry features. Zero-field-cooled measurements were made in a residual field of ca. −0.002(1) to 0.002(1) Oe based on a fluxgate response. Measurements were made on films deposited on 2-mm-diameter × 9-mm-long GC rods contained in gelatin capsules. Film mass (50−200 μg) was measured by difference using a microbalance on a Thermal Analysis Model 2050 thermal gravimetric analyzer (TGA) with a reproducibility of ±8 μg. Core diamagnetism for the films was calculated from standard diamagnetic susceptibility tables. Diamagnetic contributions corrections for the rod and holder were determined from susceptibility experiments of clean GC rods. The magnetization of the GC rods is linear with an applied field between ±50 kOe.

Thermal properties were studied on a TA Instruments Model 2910 differential scanning calorimeter (DSC) and a TA Model 2050 thermal gravimetric analyzer (TGA). The DSC is equipped with a LNCA liquid N_2 cooling accessory enabling operation between −150 and 500 °C using a modulated cell, or up to 725 °C using a standard cell. The TGA operates between ambient and 1000 °C and is located in a Vacuum Atmospheres inert atmosphere DriLab to study oxygen- and moisture-sensitive samples. Elemental analyses were performed by Atlantic Microlabs, Inc.

The $K_nCr_x[Cr(CN)_6]$ films were prepared by several techniques. Reactant solutions contained 1−5 mM of $[Cr(OH_2)_6]Cl_3$ and $K_3[Cr(CN)_6]$ dissolved in O_2-free 0.2 M KCl. Films were prepared by cycling the potential of the working electrode between −0.2 and −1.0 V for 5−20 cycles. The film-coated electrode was then rinsed with O_2-free water, placed in a solution containing 0.2 M KCl, and cycled twice between −0.2 and −1.0 V, stopping at a final potential of −0.2 V to produce an oxidized film. The film-coated electrodes were rinsed again with water and dried in a N_2 atmosphere. Reduced films were generated in a similar manner except that the potential scan was stopped at −1.0 V in the 0.2 M KCl solution. Small amounts, ca. 500 μg, of electrodeposited $K_nCr_x[Cr(CN)_6]$ could be isolated by depositing a film onto a 7-mm-diameter GC rod, stopping the scan at −0.2 V, rinsing the electrode with O_2-free water, allowing it to dry, and then removing the film by scraping the surface with a razor blade. This procedure was repeated 6−8 times to obtain 500 μg of the electrodeposted material. In some instances, ~1−3 mg quantities of the material were made by electrochemically generating a bulk precipitate in solution. Stirred, 5−10 mM solutions of both $[Cr(OH_2)_6]Cl_3$ and $K_3[Cr(CN)_6]$ favor precipitation of the bulk. After the dark-gray solids settled, the solution was decanted, and the solids were rinsed with three portions of O_2-free water and then dried under vacuum at room temperature for several hours.

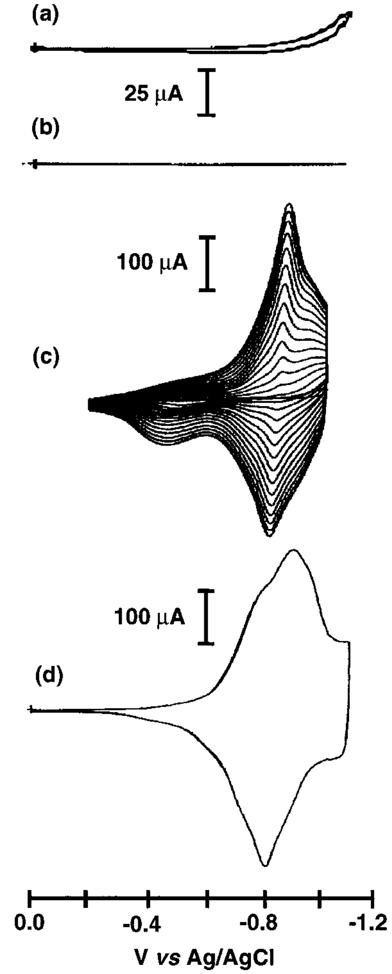

Figure 1. Voltammetric response of CG electrodes in solutions containing either (a) 2.63 mM $[Cr(H_2O)_6]Cl_3$ or (b) 1.32 mM $K_3[Cr(CN)_6]$. (c) Voltammetric response in a solution containing both 2.63 mM $[Cr(H_2O)_6]Cl_3$ and 1.32 mM $K_3[Cr(CN)_6]$. (d) Voltammetric response of the electrodeposited film in a blank 0.2 M KCl solution. Measurements made at a scan rate of 20 mV/s.

Results and Discussion

Electrodeposition of $K_nCr_x[Cr(CN)_6]$ Films. Generation of the substitutionally labile, high spin Cr^{II} species is the critical step in the deposition of $K_nCr_x[Cr(CN)_6]$ films.[6] The deposition is initiated by the irreversible reduction of $[Cr(H_2O)_6]^{3+}$ at potentials beginning at ~−0.88 V vsAg/AgCl (saturated KCl; Figure 1a). $[Cr(CN)_6]^{3-}$ is not electroactive within the potential limits used, 0.0 to −1.1 V (Figure 1b). When both $[Cr(CN)_6]^{3-}$ and $[Cr(H_2O)_6]^{3+}$ are present, however, the initial irreversible reduction evolves into a series of quasi-reversible oxidation and reduction waves (Figure 1c), that increase in current with each subsequent potential cycle until a limiting response was reached.

The voltammetric response of the film-covered electrode in a blank 0.2 M KCl solution displays a quasi-reversible wave at ca. −0.85 V vs Ag/AgCl (Figure 1d). By analogy to Prussian blue redox chemistry,[9] the observed voltammetric response is expected to correspond to the following electron-transfer reactions:

$$\mathrm{Cr^{II}[Cr^{II}(CN)_6]^{2-} \rightleftharpoons Cr^{III}[Cr^{II}(CN)_6]^{-} + e^{-}} \quad (1a)$$

$$\mathrm{Cr^{III}[Cr^{II}(CN)_6]^{-} \rightleftharpoons Cr^{III}[Cr^{III}(CN)_6] + e^{-}} \quad (1b)$$

Unlike Prussian blue films where oxidation of the metal cation and metal-centered anion are characterized by two well-resolved voltammetric waves, only one reversible wave is observed for the Cr system within the solvent limits. Infrared spectra detailed below indicate that the anion is reversibly oxidized (eq 1b) as the potential is scanned through the wave at −0.85 V. A second chemically irreversible wave is observed at the negative limit (∼−1.2 V) that may correspond to the cation reduction, eq 1a. Cycling the potential of the electrode in this potential range results in a steady decrease in peak current for the first wave at −0.85 V. The reduction of the Cr anion (eq 1b) is associated with the reversible redox process at −0.85 V, in agreement with the expectation that the cation is more easily oxidized. These results indicate that the film exists as $\mathrm{Cr^{III}[Cr^{III}(CN)_6]}$ at electrode potentials positive of reversible voltammetric wave.

The electrode surface conditions influence the morphology of the film deposited as seen in SEM and X-ray diffraction experiments discussed below. The two different morphologies, namely, amorphous spherical nodules (referred to as a), and crystalline (α) are both generated at a glassy carbon (GC) electrode surface under the same solution conditions and electrochemical potential parameters. Highly polished GC, ITO-coated surfaces, and basal plane highly oriented pyrolytic graphite (HOPG) favor a-film deposition, while “rough” GC surfaces and edge plane HOPG favor α-film deposition.

The a- and α-films are pale gray in their oxidized forms and blue-gray in their reduced forms. Both films, especially the α-film, are reasonably stable toward electrochemical degradation; the integrated peak area for an α-film decreases only ∼16% after 110 cycles. No electrochemical response is observed for either film between −0.2 and 1.2 V vs Ag/AgCl (saturated KCl; the positive potential limit of the solvent). However, a second, quasi-reversible reduction is observed beyond −1.2 V. Cycling the potential of the electrode to values more negative than 1.2 V leads to a steady decrease in peak current for the first wave.

Both $\mathrm{K_nCr_x[Cr(CN)_6]}$ film types exhibit a broad wave at ∼−0.45 V during deposition (Figure 2a,c). However, this wave is greatly diminished when the electrode is cycled in a blank KCl solution (Figure 2b,d). The electrochemical behavior of the a- and α−films differ significantly only during deposition by the intensity of this wave (∼−0.45 V) relative to the major wave (∼−0.78 V) of the film. The voltammagrams of both film types, during deposition and in blank KCl solutions, exhibit a $E_{1/2}$ between −0.80 and −0.84 V vs Ag/AgCl (saturated KCl) and have a peak-to-peak splitting, ΔE_{pp}, between 30 and 75 mV at a 20 mV/s scan rate. The absolute and relative concentrations of reactants and the scan rate affect the rate and quality of the film deposition but not the film type. The electrochemical behavior of the films in 0.2 M KCl solution is independent of pH within a pH range of 4−10. Solutions of the starting $\mathrm{Cr^{III}}$ complexes, however, decompose during attempts to adjust the pH prior to deposition.

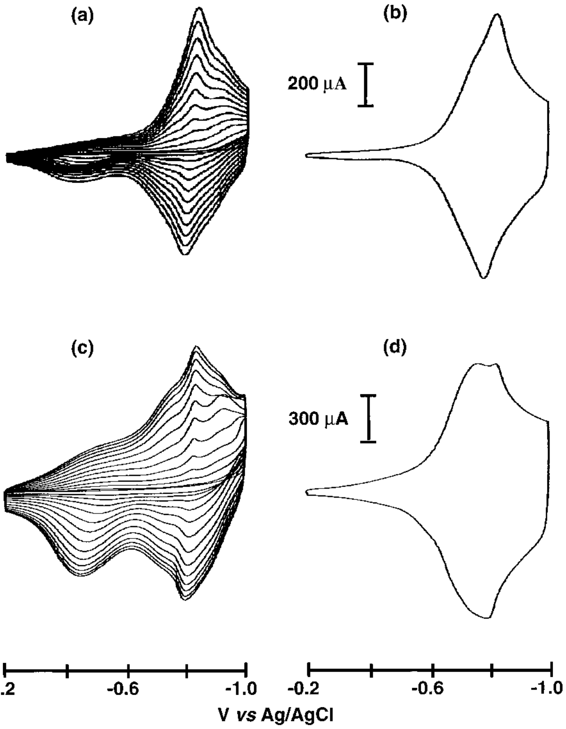

Figure 2. Voltammetric response of GC electrodes (a) during deposition of a crystalline film (type α) and (b) the first cycle of the film-coated electrode in a blank 0.2 M KCl solution. Voltammetric response of GC electrodes (c) during deposition of an amorphous film (type a) and (d) the first cycle of the film-coated electrode in a blank 0.2 M KCl solution. The solutions in (a) and (c) contain 2.63 mM $\mathrm{[Cr(H_2O)_6]Cl_3}$ and 1.32 mM $\mathrm{K_3[Cr(CN)_6]}$. The scan rate is 20 mV/s.

Charge balance during electrochemical reduction and reoxidation of the film is maintained by K^+. Thus, mobility of K^+ in and out of the Prussian blue like lattice is necessary for electroactivity of the films. Electroactivity of the films is quenched when large cations such as $\mathrm{[NBu_4]^+}$ (0.2 M) are used as the electrolyte. Attempts to measure a voltammetric response in 0.2 M potassium acetate/methanol (anhydrous) solution were also unsuccessful, demonstrating that water must also be mobile within the lattice. However, electroactivity returns when water is added to the solution. Additionally, the electroactivity of films that are vacuum-dried exhibit significantly inhibited electroactivity; the electrochemical activity can only be partially restored after soaking in 0.2 M KCl overnight.

SEM. The morphologies of the two $\mathrm{K_nCr_x[Cr(CN)_6]}$ film types are clearly distinguishable by SEM imaging of films deposited on polished GC disks (Figure 3). Images of the a-film reveals conglomerates of spherical nodules estimated to be ∼1.0 ± 0.5 μm across (Figure 3a), whereas the crystallites of the α-film are uniform well-formed cubes ∼1.0 ± 0.5 μm on an edge (Figure 3b). The electrode surface is apparent in the SEM and

---

[9] Mortimer, R. J.; Rosseinsky, D. R. *J. Electroanal. Chem.* **1983**, *151*, 133.

XPS images, indicating that the films are only one crystallite layer thick. The relative abundance of the a- and α-deposits is strongly dependent upon substrate preparation with nucleation of the α-phase favored at microscopic defects such as scratches or roughness (Figure 3c). Deliberate, albeit gentle, rubbing of a GC electrode with a 600 grit emery cloth creates parallel scratch marks, and SEM images of films deposited on this surface reveals a very dense one-to-two crystallite layer thick coverage of the α-film along the scratches and sparse coverage between the scratches.

Under the same solution and potential conditions as above, films deposited onto a HOPG working electrode yield the electrochemical response of the α-film type in Figure 2a, while films deposited on ITO-coated glass, quartz, and CaF_2 windows for optical spectroscopy gave only the electrochemical response for the a-film type in Figure 2c. SEM images of films deposited onto HOPG typically show growth of well-defined cubic crystallites of the α-film on the edge plane. In this case, no deposition occurs on the basal plane except for a sparse density of cubic crystallites at step edges. An a-film results on the rare occasion that deposition occurs on the basal plane. SEM images of films deposited onto ITO-coated surfaces also show the morphology of the a-film.

These observations suggest that the electron-transfer kinetics at the electrode surface govern the type of film deposited. Microscopic defects on the electrode surfaces, e.g., scratches or edge planes on HOPG, are apparently good nucleation sites for α-film growth. The amorphous a-films deposits on smoother surfaces of well-polished glassy carbon, ITO films, and the basal planes of HOPG.

X-ray Diffraction. The powder X-ray diffraction pattern of the a-film deposited on 7 mm GC disks is very weakly diffracting (Figure 4b); hence, it is designated to be amorphous. The weak diffraction can be assigned to a ~10% crystalline impurity. In contrast, the diffraction pattern of the α-film reveals sharp reflections (Figure 4c) identical in *d* spacing and relative intensity to a bulk precipitate generated from a more concentrated reactant solution while stirring (vide supra, Figure 4a). The sharp lines are indexed to a face-centered cubic (fcc) unit cell and the two broad peaks are from the GC substrate. The observed diffraction patterns are consistent with a cubic Prussian bluelike lattice[10] with $a = 10.41(2)$ and 10.399(3) Å for the α-film type and bulk samples, respectively, (Figure 4a,c). Films deposited onto large ITO electrodes (ca. 50 mm^2) are also weakly diffracting and additionally show very weak body-centered cubic (bcc) diffraction peaks, $a = 10.3(1)$ Å, indexed according to the selection rules as (211) and (411).

XPS. The XPS spectra of the $K_nCr_x[Cr(CN)_6]$ films clearly show that K^+ is present in the reduced forms of the films but is not detected in the electrochemically oxidized forms. Elemental chromium (574.5 eV)[11] is not detected, supporting the existence of only higher oxidation states of chromium in the films. XPS cannot resolve, however, the 2+ and 3+ oxidation states of Cr (Cr $2p_{3/2}$ = 577.5 eV) in the films or for model compounds, e.g., $K_4[Cr^{II}(CN)_6]$, $K_3[Cr^{III}(CN)_6]$, $Cr^{III}Cl_3$, and

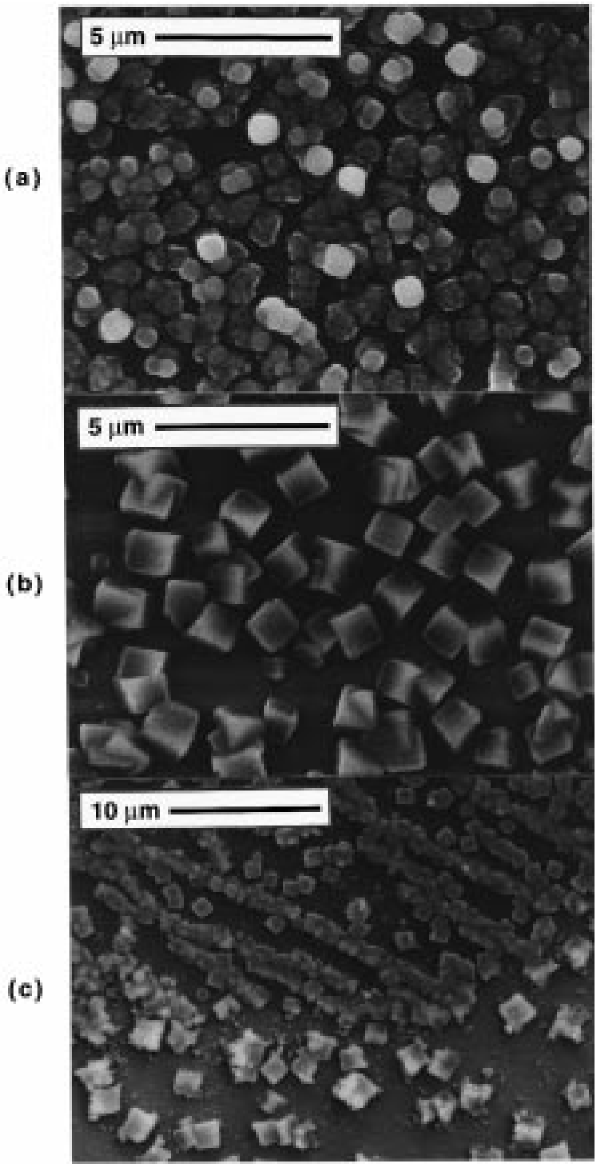

Figure 3. SEM images of (a) the a-film, (b) the α-film, and (c) mixtures of a- and α-films with α-crystallites formed at scratches on an electrode. All images taken at 20 kV.

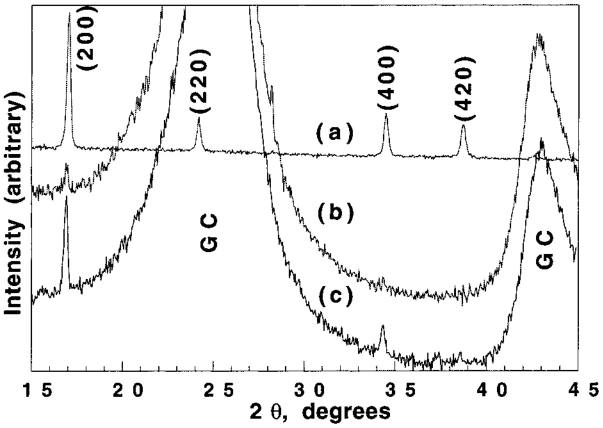

Figure 4. X-ray diffraction patterns of the (a) crystalline bulk sample, (b) amorphous a-film type, and (c) crystalline α-film. The broad peaks are the GC substrate.

---

[10] (a) Entley, W. R.; Treadway, C. R.; Girolami, G. S. *Mol. Cryst. Liq. Cryst.* **1995**, *273*, 153. (b) Buser, H. J.; Schwarzenbach, D.; Petter, W.; Ludi, A. *Inorg. Chem.* **1977**, *16*, 2704. (c) Weiser, H. B.; Milligan, W. O.; Bates, J. B. *J. Phys. Chem.* **1942**, *46*, 99.

[11] *Handbook of X-ray Photoelectron Spectroscopy*; Muilenberg, G. E., Ed.; Perkin-Elmer Corp.: Eden Prarie, MN, 1978.

$Cr^{II}_2(OAc)_4$ (Cr $2p_{3/2}$ = 576.2, 576.2, 576.4, 576.8 eV, respectively), consistent with the literature.[11] Furthermore, these model compounds are also poor for determining the relative stoichiometry as they do not provide reliable element ratios in the films. Due to the small amounts of samples scraped off the electrodes (<2 mg), meaningful elemental analyses could not be made.

Oxygen will oxidize the Cr^{II} sites, but it is not significantly incorporated into the film. The oxygen levels in the XPS spectra do not measurably increase when the films are exposed to air for 1−2 days. The oxygen present in the XPS spectra is found, on uncoated electrodes, to be associated with surface oxides,[12] and trace amounts of alumina and silica remaining on the electrode surface from fabrication and polishing.

Infrared Spectroscopy. The infrared spectra of the two film types can be used to determine the relative ratio of anionic sites occupied by Cr^{II} (υ_{CN} = 2072s cm^{-1}; half-width at half-height ~ 90 cm^{-1}) and Cr^{III} (υ_{CN} = 2185m cm^{-1}; half-width at half-height ~ 20 cm^{-1})[5,6] but is insensitive to the oxidation state of the chromium in the cationic sites or the film type. A fully reduced (only υ_{CN} = 2072 cm^{-1} present) film deposited on an IR-transparent (1200−4000 cm^{-1}) ITO-coated CaF_2 window, can be fully oxidized (only υ_{CN} = 2185 cm^{-1} present) in ca. 55 min by air exposure (Figure 5a). However, electrochemical oxidation does not fully oxidize all the $[Cr^{II}(CN)_6]^{4-}$ in the film as determined by IR analysis. A small amount of $[Cr^{II}(CN)_6]^{4-}$ (~2%) remains even after holding the potential at −0.20 V for 12 h (vide infra). Reasons for this include the possibility that the Cr^{3+}:$[Cr(CN)_6]^{n-}$ ratio is not precisely 1:1, thus requiring some $[Cr^{II}(CN)_6]^{4-}$ to balance charge or the possibility that some sites in the film are electrochemically inaccessible.

Stoichiometry. The absolute stoichiometry of the films is elusive. As discussed above, the absolute Cr^{II}/Cr^{III} ratio cannot be determined from XPS data; however, the Cr^{II}/Cr^{III} ratio for the anionic sites can be determined from the ratio of the integrated areas of the υ_{CN} bands in the IR spectra. These ratios are normalized to the two extreme cases, i.e., all $[Cr^{II}(CN)_6]^{4-}$ and all $[Cr^{III}(CN)_6]^{3-}$, by air oxidation of a single film (Figure 5a). Using these data, the normalized peak area of each anion is plotted as a function of the ratio of the integrated peak areas (Figure 5b). An electrochemically oxidized film held at −0.20 V for 12 h exhibits a $[Cr^{II}(CN)_6]^{4-}/[Cr^{III}(CN)_6]^{3-}$ integrated area ratio of 0.15. This ratio on the experimental curve (Figure 5b) corresponds to 0.98 $[Cr^{III}(CN)_6]^{3-}$:0.02 $[Cr^{II}(CN)_6]^{4-}$ for the above electrochemically oxidized film. The data for 1.0 correspond to $[Cr^{II}(CN)_6]^{4-}$ for the reduced film.

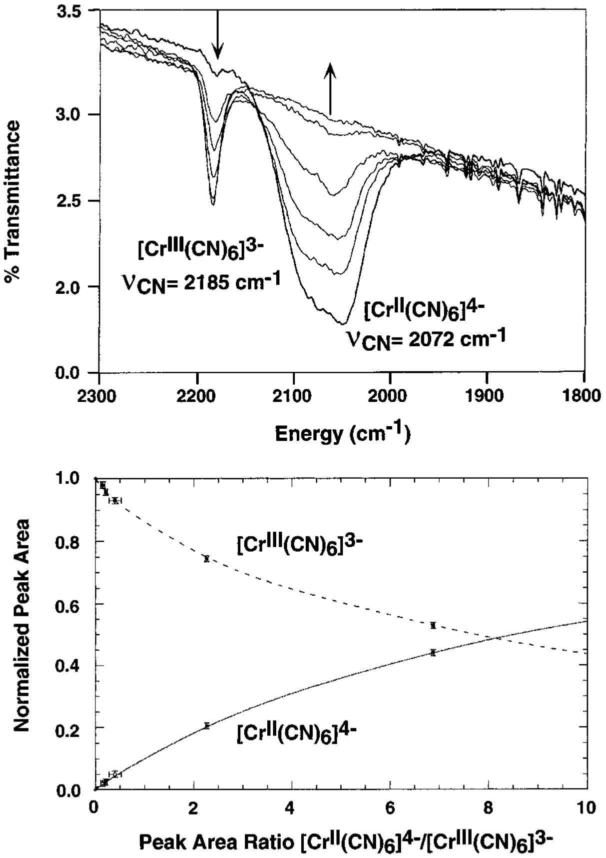

Figure 5. (a) IR spectra of the υ_{CN} region for an electrode-posited film cycled to −1.0 V and allowed to air oxidize. Spectra were recorded over a period of 55 min. (b) Normalized peak area vs peak area ratio. The lowest peak area ratio (0.15) point for $[Cr^{II}(CN)_6]^{4-}$ corresponds to a film electrochemically oxidized at −0.2 V for ca. 12 h (T_c = 230 K), while the lowest peak area ratio (0.40) point for $[Cr^{III}(CN)_6]^{3-}$ corresponds to a film electrochemically oxidized at −0.2 V for ca. 4 min (T_c = 260 K).

The next issue is determining the appropriate cationic Cr^{n+} oxidation state and the quantity of cations sites necessary to balance the total anionic charge. The assumption is made that the cationic site is in a fully oxidized Cr^{III} state when the films are electrochemically oxidized. Supporting this assumption are the following observations: no electrochemistry is observed between −0.20 and +1.20 V for the films, and hence the remaining $[Cr^{II}(CN)_6]^{4-}$ ions (seen in the IR) must be trapped due to charge balance requirements. The presence of other cations not easily detectable by spectroscopy, i.e., H^+ or H_3O^+, is unlikely since there is no pH dependence upon the electroactivity of the films. Since K^+ or other cations are not detected by XPS in the electrochemically oxidized films, only Cr^{III} cations are present to balance the total anion charge, giving a stoichiometry of $Cr^{III}_{1.00}[Cr^{III}(CN)_6]_{0.98}[Cr^{II}(CN)_6]_{0.02}$.

The Cr^{III} cation site is assumed to be fully reduced to Cr^{II} when the film is held at its most reducing potential, −1.0 V. This is substantiated by two observations: (1) the deposition of the material does not occur unless Cr^{II} cation species are present in solution; thus, the first material formed is $Cr_3^{II}[Cr^{III}(CN)_6]_2$ as isolated in the bulk synthesis.[5] (2) However, for films in the electrochemically reduced state at −1.0 V, only the $[Cr^{II}(CN)_6]^{4-}$ anion is observed by IR υ_{CN} absorption. Therefore both sites are ultimately reduced to Cr^{II} after deposition onto the electrode with K^+ balancing the charge in accord with the XPS data. The K^+-containing reduced films were estimated to be $K_{2.0}Cr^{II}[Cr^{II}(CN)_6]$ from the aforementioned υ_{CN} IR-intensity analyses. These stoichiometries are comparable to previously reported bulk analysis of similar materials reported in Table 1.

When the potential of the film-coated electrode is held at −0.2 V for ca. 4 min, there is evidence for residual $[Cr^{II}(CN)_6]^{4-}$ by the IR analyses. The $[Cr^{II}(CN)_6]^{4-}/$

---

(12) McCreery, R. L. *Electroanal. Chem.* **1991**, *17*, 221.

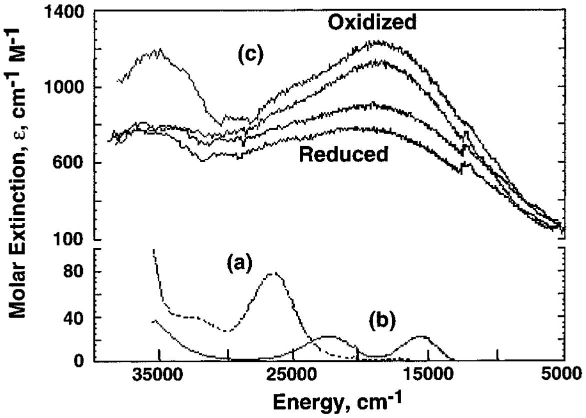

Figure 6. Optical spectra of solutions of (a) $K_3[Cr(CN)_6,]$ (b) $[Cr(H_2O)_6]Cl_3$, and (c) an electrodeposited $K_nCr_x[Cr(CN)_6]$ film on an ITO-coated quartz slide subjected to oxidizing and reducing potentials. The discontinuity at 1200 cm^{-1} is due to a change in the detector.

$[Cr^{III}(CN)_6]^{3-}$ integrated area ratio for these films is 0.40. This corresponds to 0.93 $[Cr^{III}(CN)_6]^{3-}$:0.05 $[Cr^{II}(CN)_6]^{4-}$. In this case the cationic $Cr^{III}(NC)_6$ site may not be all Cr^{III}. This difference, although small, has a significant effect on the magnetic ordering temperature (vide infra).

UV–Vis–NIR. The optical spectrum of the $K_nCr_x[Cr(CN)_6]$ films exhibit a broad absorption in the visible region that is too intense to be simple combination of the constituent ions (Figure 6). This band is stronger for the electrochemically oxidized films, $\lambda_{max} \sim 18\,800$ cm^{-1} ($\epsilon \sim 1280$ cm^{-1} M^{-1}), than for the reduced films, $\lambda_{max} = 20\,200$ cm^{-1} ($\epsilon \sim 870$ cm^{-1} M^{-1}). The 18 800 cm^{-1} absorption band of the oxidized film is consistent with an expected intervalence charge transfer (IVCT)[13] which, consistent with the IR data, supports the presence of some residual Cr^{II}. In addition to these very broad absorption bands is another strong band at 35 500 cm^{-1} ($\epsilon \sim 1180$ cm^{-1} M^{-1}) for the oxidized film and another band 36 200 cm^{-1} ($\epsilon \sim 770$ cm^{-1} M^{-1}) for the reduced film that are not seen in the spectra of the constituent ions. Further work is required to assign these bands.

The two strong absorption bands of the oxidized film are assigned in a manner similar to those of Prussian blue and related compounds.[14] The 18 800 cm^{-1} absorption is assigned to the $t_{2g} \rightarrow t_{2g}'$ IVCT transition. The 35 500 cm^{-1} absorption is assigned to the $t_{2g} \rightarrow e_g'$ IVCT transition, which is typically weaker in oscillator strength than the lower energy transition. The separation of these bands, 16 700 cm^{-1}, should then reflect the crystal field splitting, Δ_0, of $[Cr^{III}(NC)_6]^{3+}$. This value is consistent with Δ_0 found in $[Cr^{III}(H_2O)_6]^{3+}$ of 17 000 cm^{-1}.[15a]

In reduced films (where all chromium is present as Cr^{II}) an intervalence charge-transfer (IVCT) band is not expected. In this situation, however, the two Cr^{II} sites are in different spin states. The $[Cr^{II}(CN)_6]^{4-}$ is low spin, $S = 1$ (strong ligand field site), and the $[Cr^{II}(NC)_6]^{2+}$ is high spin, $S = 2$ (weak ligand field site). This difference in the local electronic structure can still lead to intermetallic charge transfer as reported for several examples of $M^{II}-Fe^{II}(CN)_6$ (M = Mn, Co, Ni, Cu) Prussian blue like materials.[14,16] Therefore, if the absorptions at 20 200 and 36 200 cm^{-1} are similarly assigned to $t_{2g} \rightarrow t_{2g}'$ and $t_{2g} \rightarrow e_g'$ intermetallic charge-transfer transitions, respectively, then their separation reflects a Δ_0 of 16 000 cm^{-1} of $[Cr^{II}(NC)_6]^{2+}$. This decrease in Δ_0 in comparison to $[Cr^{III}(NC)_6]^{3+}$ is anticipated for the lower oxidation state and is comparable to the Δ_0 of 15 500 cm^{-1} reported for $[Cr^{II}(NCMe)_6]^{2+}$.[17] These Δ_0's are as expected significantly lower than the 26 600 cm^{-1} Δ_0 for $[Cr^{III}(CN)_6]^{3-}$[18a] and ~22 000 cm^{-1} Δ_0 for $[Cr^{II}(CN)_6]$.[4-18b]

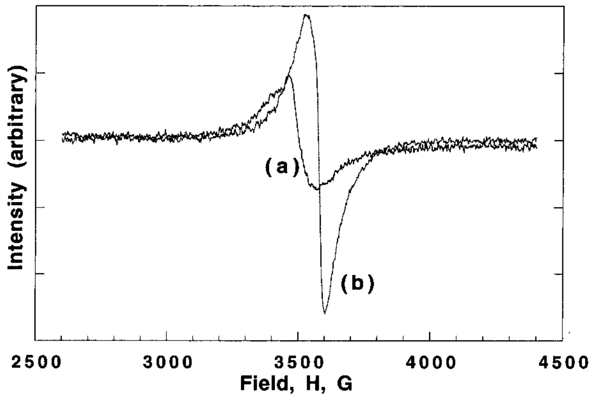

Figure 7. EPR derivative curve spectrum of an oxidized $K_nCr_x[Cr(CN)_6]$ film at (a) 300 K (intensity ×1000) and (b) 188 K, above and below the T_c.

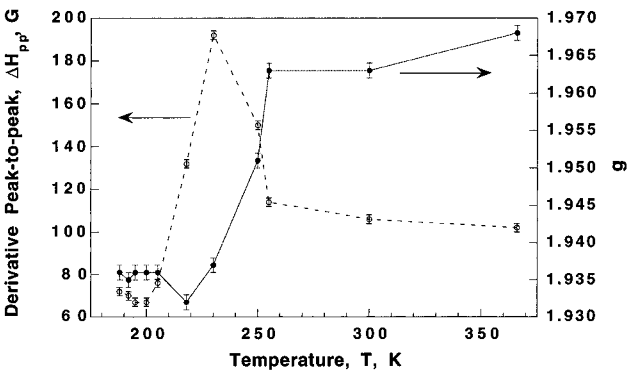

Figure 8. Derivative peak-to-peak, ΔH_{pp}, separation (○) and observed Landé g values (●) of an oxidized a-film around the T_c ($\nu = 9.659$ GHz).

EPR. The $K_nCr_x[Cr(CN)_6]$ films exhibit a single resonance above T_c which increases in peak height intensity by 3 orders of magnitude as it is cooled into its magnetic state (Figure 7). (Blank GC rods did not exhibit detectable signals under the same conditions.) The spectra shown are for an a-film in an oxidized state with $T_c \sim 230$ K. As the film is cooled through T_c, the Landé g value drops from 1.963(1) (300 K) to 1.936(1) (below T_c; Figure 8). This is characteristic of an ordered magnetic material orienting its internal field, H_{int}, with the applied field, H_0.[19a] This shift in resonance field gives an H_{int} of 49 G. The peak-to-peak separation,

---

(13) Robin, M. B.; Day, P. *Adv. Inorg. Chem Radiochem*, **1967**, *10*, 247.

(14) Braterman, P. S. *J. Chem. Soc. A* **1966**, 1471.

(15) Figgis, B. N. *Introduction to Ligand Fields*; John Wiley-Interscience: New York, 1966; (a) Chapter 9, (b) p 244. (c) Chapter 5.

(16) Robin, M. B. *Inorg. Chem.* **1962**, *1*, 377.

(17) Buschmann, W. E.; Miller, J. S. *Eur. J. Chem.*, in press.

(18) (a) Alexander, J. J.; Gray, H. B. *J. Am. Chem. Soc.* **1968**, *90*, 4260. (b) Estimated from empirical parameters.[15b]

ΔH_{pp}, increases around T_c and then decreases to an overall smaller value in its ordered magnetic state. This reduction in ΔH_{pp} is due to strongly coupled magnetic interactions resulting in "exchange narrowing" (Figure 8).[19b]

Magnetic Susceptibility. Magnetization data are corrected on a per-mole basis using the aforementioned molecular formulas. Identical formulas are assumed for both the a- and α-film types as (1) there are no indications of any major differences other than crystallinity and morphology and (2) films deposited under identical solution and potential conditions have (a) indistinguishable IR spectra and (b) the XPS data are qualitatively the same. After the film-coated GC rods are used in the susceptibility measurements, they are analyzed for water content by TGA up to 475 °C. Water loss occurs between 55 and 100 °C. Above 120 °C the films decompose with a continual weight loss throughout the temperature range. Water content based on these measurements is approximately 0.5 mol of water/formula unit and is included in the diamagnetic susceptibility corrections, i.e., -92×10^{-6} (oxidized film) and -121×10^{-6} (reduced film) emu/mol. Fits to the Curie−Weiss expression above T_c to obtain a θ value were unreliable due to extreme scatter in the high-temperature data resulting from the small mass of the films relative to the GC substrate.

The temperature dependence of the magnetization, $M(T)$, was measured in a 5 Oe applied field on warming after cooling in various dc fields [0 ± 0.002 (ZFC), ±5, and ±10 Oe] for both oxidized and reduced a-films (Figure 9), and α-films (Figure 10). The ordering (critical) temperature T_c was determined by extrapolating the initial slope of the rise in magnetization to the temperature axis and was the same for both films. The T_c (135 K) was smaller for the reduced films than for the oxidized films (230−260 K) with the greatest T_c value corresponding to the less than fully oxidized films, consistent with the literature.[6]

The $M(T)$ data also reveal the "freezing-in" of the magnetization after cooling from above T_c to 20 K in a negative applied dc field. The curves obtained on cooling in fields of equal strength, but opposite sign, are nearly symmetric about the zero field cooled (ZFC) magnetization. ZFC measurements result in a positive magnetization reduced by more than an order of magnitude from the FC data, but both the ZFC and FC magnetization data converge to the same T_c. A dc field of +5 Oe applied upon warming to a sample cooled in a negative field (i.e., $H_{dc} = -5$ or -10 Oe) is insufficient to "flip" the spins. This negative (reversed) magnetization is observed in all (ca. 20) $K_nCr_x[Cr(CN)_6]$ films studied. Fields as high as about 100 Oe are necessary, at 20 K, to reverse the negative magnetization for samples cooled in −5 Oe.

Hysteresis is observed for all $K_nCr_x[Cr(CN)_6]$ films (a or α, oxidized or reduced) studied and depends on the temperature at which it was measured, the degree of crystallinity, and the oxidation state of the film. The 20 and 150 K coercive field, H_{cr}, and the 3 kOe magnetization at 20 K, M_s, for a- (Figure 11a) and α-films (Figure 11b), each with different oxidation state, are listed in Table 2.

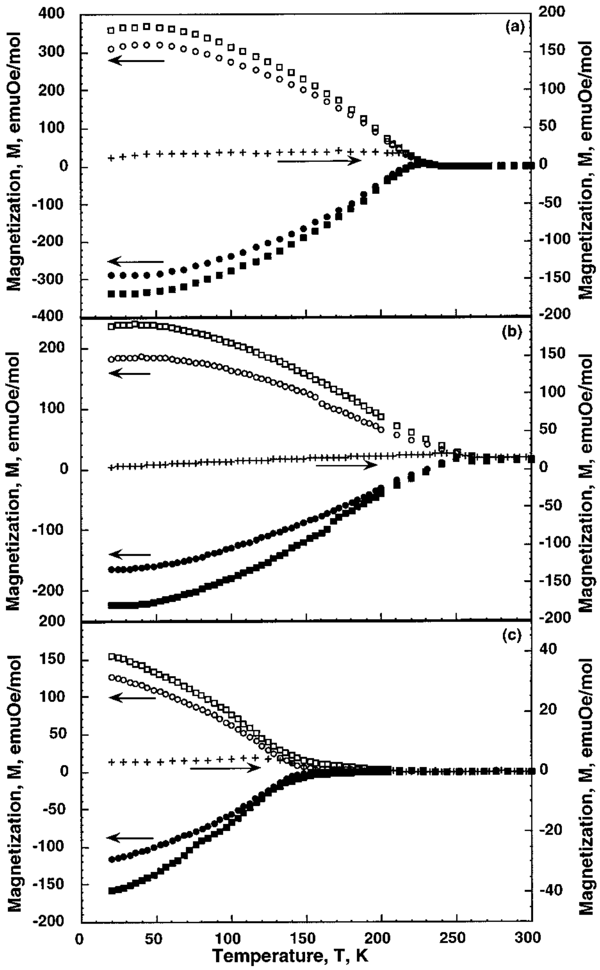

Figure 9. Temperature-dependent magnetization of the a-film, ZFC (+) and FC in 5 Oe (○), −5 Oe (●), 10 Oe (□), −10 Oe (■) after (a) 12 h oxidation (−0.2 V), (b) 2 min oxidation (−0.2 V), and (c) 5 min reduction (−1.0 V). All data collected upon warming in a 5 Oe field.

The coercive field at 20 K is consistently larger for the a- than for the α-films, even though the differences are relatively small (≤10 Oe for oxidized films and up to 240 Oe for reduced films). Differences in H_{cr} up to 730 Oe arise from variations in oxidation state. The H_{cr} is larger for further reduced films, as they possess a higher Cr^{II} content. The small magnetization values observed at 3 kOe suggest a small saturation magnetization, consistent with previous reports.[5,6] The low value of the magnetization is a consequence of the relatively large amount of $Cr^{III}-CN-Cr^{III}$ moieties in which the spins on adjacent sites compensate each other. At higher fields there are signatures of unusual $M(H)$ behavior presently under further investigation.

The ac magnetic susceptibility (χ_{ac}) of the reduced films exhibit both in-phase (χ') and out-of-phase (χ'') components (Figure 12). Both $\chi'(T)$ and $\chi''(T)$ undergo a rapid increase in the temperature range where the dc measurements show an onset of the magnetization. The presence of χ'' demonstrates that these films are lossy and have an uncompensated moment. χ' has a broad maxima at ~120 K.

Hence, all films have magnetic ordering, with a T_c independent of the crystallinity but strongly dependent

---

(19) Bencini, A.; Gatteschi, D. *Electron Paramagnetic Resonance of Exchange Coupled Systems*; Springer-Verlag: New York, 1990; (a) p 162, (b) p 129.

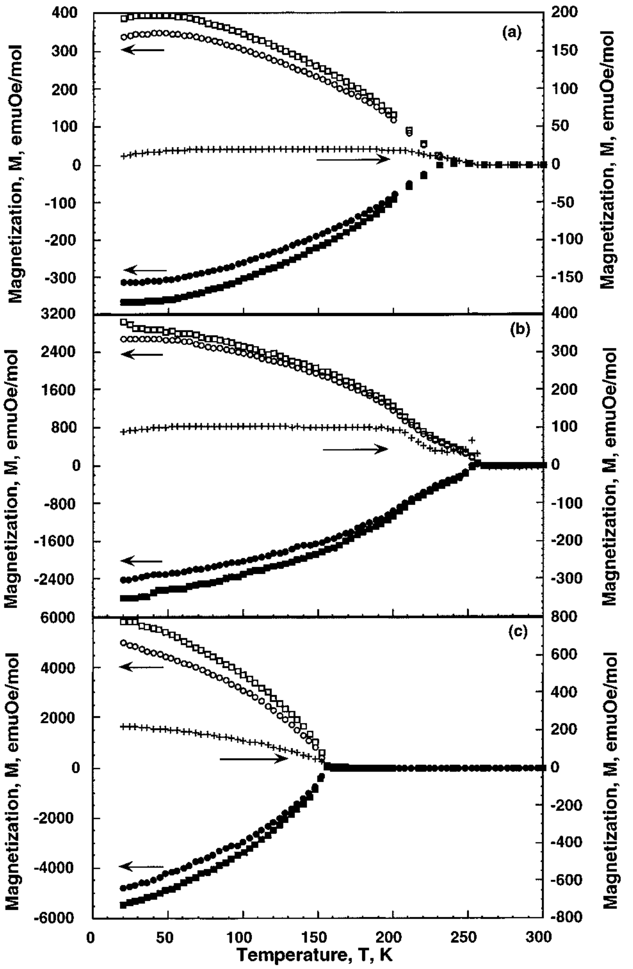

Figure 10. Temperature-dependent magnetization of the α-film, ZFC (+) and FC in 5 Oe (○), −5 Oe (●), 10 Oe (□), −10 Oe (■) after (a) 12 h oxidation (−0.2 V), (b) 5 min oxidation (−0.2 V), and (c) 5 min reduction (−1.0 V). Air contamination caused excessive oxidation in this sample and results in the higher T_c shown. (Other samples reduced under the same conditions condition have a 135 K T_c but were not subjected to all five susceptibly measurements.) All data collected upon warming in a 5 Oe field.

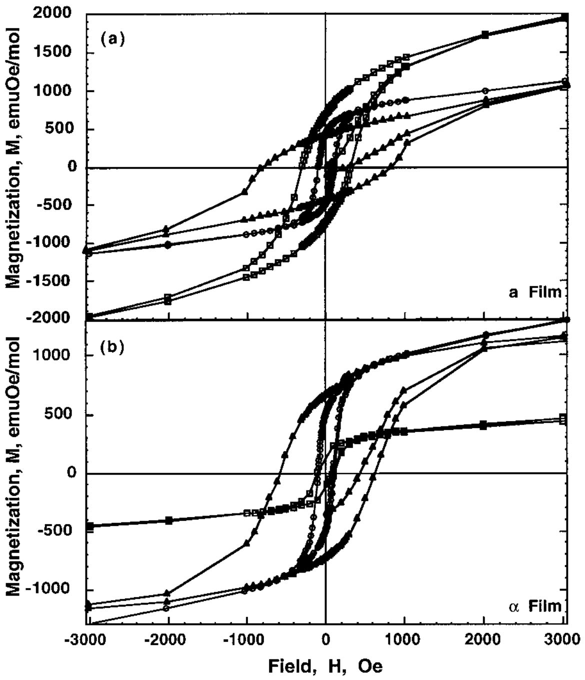

Figure 11. Field dependence of the a- (a) and (b) α-films at 20 K after (○) 12 h oxidation (−0.2 V), (□) 2 min oxidation (−0.2 V), and (△) 5 min reduction (−1.0 V).

on the oxidation state and have a robust negative magnetization "frozen-in" by cooling through the transition in a small negative applied field. The hysteresis curves revealed that H_{cr} is only weakly dependent on crystallinity and strongly dependent on the oxidation state. Dynamic susceptibility studies provided χ_{ac} data consistent with the magnetization and hysteresis curves.

To account for these effects, we address the nature of the possible spin configurations and the magnetic interactions present in these systems. Cr^{II} ions can be either high-spin ($S = 2$) in a weak ligand {i.e., $[Cr^{II}(NC)_6]^{2+}$} environment or low-spin ($S = 1$) for a strong ligand {i.e., $[Cr^{II}(CN)_6]^{4-}$} environment while Cr^{III} can only be $S = 3/2$. The coupling between the unpaired d-orbital spins of two metal ions bridged by a CN group is ferromagnetic if these orbitals are orthogonal but antiferromagnetic if there is an overlap of the orbitals.[5] For completely oxidized $K_nCr_x[Cr(CN)_6]$ films the adjacent spin sites have three unpaired electrons in the t_{2g} orbitals and should couple antiferromagnetically due to significant orbital overlap. The number of unpaired electrons on adjacent sites is never equal in completely reduced films; thus, an uncompensated moment, albeit small, leading to magnetic ordering is expected. The experimental data for the $K_nCr_x[Cr(CN)_6]$ films are consistent with ferrimagnetic behavior, similar to several other Prussian-blue analogues.[4−6]

Another magnetic interaction that plays a crucial role in these systems arises from the magnetocrystalline anisotropy. Octahedral, low-spin d^4 $[Cr^{II}(CN)_6]^{4-}$ has a triply degenerate $^3T_{1g}$ ground state. However, distortions of the octahedral symmetry around the Cr^{II} ion leads to the removal of the orbital degeneracy and some single-ion anisotropy, SIA. (Such distortions are known to occur in the isoelectronic $[Mn^{III}(CN)_6]^{3-}$, where the two axial M-CN bonds are ca. 0.01 Å shorter than the equatorial ones.[17]) Similarly, distortions of the octahedral environment breaks the orbital degeneracy for high-spin Cr^{II}.[16] The anisotropy of the Cr^{III} ion is likely negligible due to the nondegenerate $^4A_{2g}$ ground state. The presence of both low- and high-spin Cr^{II} and Cr^{III} led to variations in the strength of the zero-field splitting, *D*, arising from the SIA. We propose that SIA is responsible for the negative (reversed) magnetization observed in the *M*(*T*) curves. The anisotropy creates a preferred (easy) axis of spin orientation. Hence, upon cooling through T_c the system orders such that the spins are "locked" in their preferred direction, parallel to the field, if the direction of the field is the same as the easy axis, or at the smallest angle with the field when the two directions do not coincide. When a field is applied in the opposite direction, the SIA creates a barrier against flipping the spins to align them along or close to the new direction, such that a greater field is necessary to overcome the strength of the anisotropy.

The interplay between local variations in magnetic anisotropy, exchange coupling, and the structural disorder (crystallographic defects, grain boundaries, etc.) is proposed to be responsible for the hysteretic behavior of the $K_nCr_x[Cr(CN)_6]$ films. The domain-wall pinning

Table 2. Summary of the Magnetic Properties for Both the Fully Oxidized and Reduced A- and α-Films

	T_c, K	M_s, emu Oe/mol[a]	H_{cr}, Oe (20 K)	H_{cr}, Oe (150 K)	film mass, μg[b]
$Cr^{III}[Cr^{III}(CN)_6]_{0.98}[Cr^{II}(CN)_6]_{0.02}$[c]					
amorphous	230	1130	100	40	53
crystalline	230	1300	90	40	51
$K_{2.0}$ $Cr^{II}[Cr^{II}(CN)_6]$[d]					
amorphous	135	1070	830		65
crystalline	135	1160	590		109
$Cr^{III}[Cr^{III}(CN)_6]_{0.95}[Cr^{II}(CN)_6]_{0.05}$[e]					
amorphous	260	1980	120	70	113
crystalline	260	450	110	70	214

[a] Saturation values at 20 K and 3 kOe. [b] Values are reliable to ±8 μg of sample mass. [c] Oxidized films (−0.20 V, 12 h). [d] Reduced films (−1.00 V, 5 min). [e] Oxidized films (−0.20 V, < 5 min).

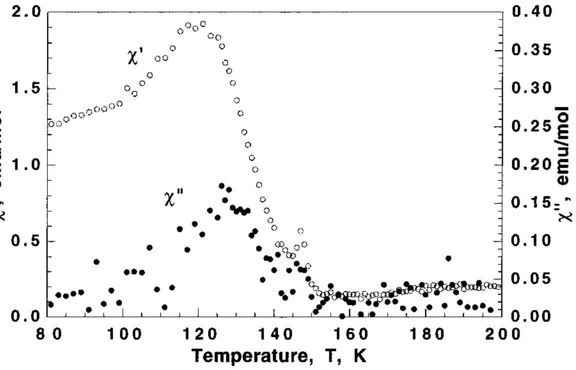

Figure 12. Ac susceptibility of the reduced α-film, χ′ (○) and χ″ (●). The measurement was made using a 3.5 Oe ac field amplitude with a 2 Hz driving frequency and a dc field of 0 ± 0.05 Oe. The sample was cooled in a 5 Oe dc field, the dc coil quenched, and data collected upon warming.

sites are structural defects or regions with local variation of the domain-wall energy, which, in turn, depends on the magnetocrystalline anisotropy and exchange coupling.[20] In this model, the coercivity of the amorphous films is larger than that of the crystalline films due to the larger number of defects in the a-films. These defects arise from lattice disorder (seen in the poor X-ray diffraction, Figure 4) and grain boundaries between the spherical nodules that make up the crystallites (Figure 3a). Similarly, variations in magnetocrystalline anisotropy and/or exchange coupling are likely responsible for the differences between the coercivities of the films.

Previous studies claimed that samples with higher Cr^{III} content exhibit larger critical temperatures, arguing that the $Cr^{III}-CN-Cr^{III}$ moieties eliminate vacancies, increasing the number of nearest neighbors and, hence, T_c.[6] The T_c of the Cr^{III}-rich (oxidized) films are about twice that of the reduced, Cr^{II}-rich, films. This is probably due in part to the strength of the exchange, J, which is likely to be larger when the Cr^{III} ions are present, due to the larger overlap through the ligand orbitals.[15c]

Small differences in the Cr^{II} content of Cr^{III}-rich films lead to quantifiable variations in T_c. A 3% increase in the $[Cr^{II}(CN)_6]^{4-}$ content in the oxidized films results in ~30 K increase in T_c. Further increases in $[Cr^{II}(CN)_6]^{4-}$, however, decrease T_c. The identification of an optimum Cr^{III}:Cr^{II} content maximizing T_c deserves further investigation.

Usually structural disorder hinders the occurrence of long-range magnetic order.[21] Since this is not evident, it raises the question of whether there is a mixture of crystalline and amorphous regions in every sample, with only one phase being responsible for the magnetic response in films of similar oxidation state. Examining more closely the X-ray data, one notices that the amorphous film has small features where the crystalline film has clear peaks. The ratio of the peak areas between a- and α-films suggests ~10% crystallinity of the amorphous film. Comparing these differences to the much larger difference in M_s (e.g., 4:5, 2:1, etc.) suggests that the magnetic response cannot be solely caused by the crystalline regions as the amorphous phase has a substantial contribution. Hence, we suggest that the magnetic domains are smaller than the size of the structurally ordered regions in both a- and α-films leading to similar T_c's, regardless of crystallinity.

Conclusion

Thin films (1−2 μm) of $K_nCr_x[Cr(CN)_6]$ can be electrodeposited on to GC electrodes or ITO electrodes in either amorphous or crystalline forms. The magnetization data reveal magnetic ordering, with a T_c as high as 260 K, independent of the crystallinity but strongly dependent on the oxidation state, and showing robust negative magnetization “frozen-in” by cooling through the transition in a small negative applied field. Hysteresis curves reveal that H_{cr} is weakly dependent on crystallinity but strongly dependent on the oxidation state with reduced films having greater coercive fields.

The coercivity correlates with both the structural disorder and the local variations in domain-wall energy due to the nonuniformities in exchange and magnetocrystalline anisotropy. The T_c does not always correlate with the Cr^{III} content, in partial agreement with previous reports. Further studies are needed to explain the independence of the critical temperature on structural disorder. The observed negative magnetization can be accounted for by SIA.

Acknowledgment. We gratefully acknowledge the guidance provided by Prof. M. Verdaguer and T. Mallah (Universite Pierre et Marie Curie) and the support from the U. S. Department of Energy Grant Nos. DMS DE FG 02-86BR45271, DMS DE FG 03-93ER45504, and DE FG02-96ER12198, the Office of Naval Research, and the NSF Grant Nos. CMS 9413498 and CHE-9320478 for the XPS and SQUID instruments.

CM970773V

---

(20) McCurrie, R. A. *Ferromagnetic Materials*, Academic Press: New York, 1994; Chapter 1.

(21) Epstein, A. J.; Miller, J. S. *NATO ASI, E321* **1996**, 415.